PCCP

RSC Publishing

PAPER

View Article Online
View Journal | View Issue

Tunable electronic and dielectric behavior of GaS and GaSe monolayers

Cite this: *Phys. Chem. Chem. Phys.*, 2013, **15**, 7098

Yandong Ma, Ying Dai,* Meng Guo, Lin Yu and Baibiao Huang

Received 18th January 2013,
Accepted 13th March 2013

DOI: 10.1039/c3cp50233c

www.rsc.org/pccp

Here we present first-principles calculations to investigate systematically the electronic behavior and the electron energy low-loss spectra (EELS) of monolayer, bilayer, four-layer, and bulk configurations of periodic GaX (X = S, Se), as well as the effect of mechanical strain on the electronic properties of the GaX monolayer. We predicate that the GaX monolayer is a semiconductor with an indirect band gap, however, the difference between the direct and indirect gaps is so small that electrons can transfer easily between this minimum with a small amount of thermal energy. Owning to strong surface effects, the electronic and dielectric properties of GaX vary drastically with number of layers in a sheet. In detail, the band gap increases from multilayer-to-single layer and EELS shifts towards larger wavelengths with a decrease in the layer thickness. Moreover, we demonstrate that the band gaps of GaX monolayers can be widely tuned by mechanical deformation, making them potential candidates for tunable nanodevices. The present study provides theoretical insight leading to a better understanding of these novel 2D structures.

I. Introduction

Successful exfoliation of two-dimensional (2D) materials has opened up new exciting possibilities for development of the next generation of nanoelectronic devices.[1–6] They typically possess distinct properties from their three-dimensional (3D) counterparts. Despite the intensive research interest, the variety of experimentally realized freestanding 2D materials still remains relatively low.[2–6] Obviously, as the first prototype of layered structures, graphene has predominated as the most widely studied 2D system for its unique electronic structure. One such aspect is using its enormous surface area and electron conductivity as a platform for hydrogen storage.[7,8] Nevertheless, for use in nanoelectronic devices, the lack of an intrinsic band gap has constituted a formidable hurdle.[9–13] In this context, the search for new classes of other new 2D materials that may offer new opportunities for specific properties and applications is of both fundamental interest and technological significance.

GaS and GaSe have been studied in previous literature.[14,15] It is interesting that, rather recently, a stable class of 2D metal dichalcogenide (MD) materials, GaX (X = S, Se) monolayers, has been synthesized experimentally,[16–18] opening a fascinating new chapter in nanoelectronic applications. Unlike previously studied MDs, such as VS_2, MoS_2 and NbS_2 monolayers,[6,19,20] GaX monolayer comprises light elements only. It was pointed out that the mechanically robust GaX monolayers are perfect candidates for use in field-effect transistors (FETs) enabling substitution of organic-based FETs.[17] Aside from these intriguing features, other virtues GaX monolayer possessed are the thermal stability and the absence of dangling bonds, rendering them promising for nanophotonic devices.[18] Moreover, the GaX monolayer is also promising for obtaining nanotubes and other nanomaterials which show confinement effects in their electronic and optical properties. And, as we know, many reports are available in the literature about the electronic properties of the bulk GaX.[14,15,21,22] However, as an emerging family of 2D materials, the properties of GaX monolayers are still in the early stages of exploration and are fascinating the scientific communities. In this sense, for further development and applications, a systematic theoretical understanding of these monolayers would be highly desirable.

Another important challenge for development of GaX monolayer-based electronics is that materials made for devices should be large and uniform. Note that all synthesis methods produce not only monolayer but all types of flakes, from few-layer to those approaching bulk-like materials.[16] A rapid and unambiguous method for determining the number of layers in a sheet is vital to accelerate research and exploration of their properties. Researchers have attempted to develop efficient ways [*i.e.*, transmission electron microscopy (TEM), coupled with flake

School of Physics, State Key Laboratory of Crystal Materials, Shandong University, Jinan 250100, People's Republic of China. E-mail: daiy60@sina.com

edge analysis, electron diffraction, or/and electron energy loss spectroscopy (EELS)] to identify various numbers of the layers of specimens.[23–25] Among them, EELS is considered to be a powerful technique which correlates the atomic and electronic structure.[24,25] Given the significant contrast in electronic and dielectric properties among various layered materials, EELS can be a practical technique to investigate the variation in properties of these sheets with respect to the number of layers. However, up to now, there is a notable absence of a detailed investigation of the effect of thickness variation on the dielectric response as well as the EELS in GaX.

On the other hand, advanced applications often require materials with tunable and reversible electronic properties which can be deliberately modulated by external control parameters.[26] Therefore, tuning and controlling the electronic properties of GaX monolayer—for their potential application in electromechanical devices, tunable photodetectors, and lasers—are desirable. An applied electronic field or light offers a novel way to modify the electronic properties over a wide range.[27,28] As an example, for graphene, it has been shown that bilayer applied by vertical electronic field opens a small band gap.[29,30] These techniques are promising but suffer from a lack of practical applicability. For instance, the band gap of a single layer remains unaffected by the external electronic field and can only be modulated for the two or more layers.[31] As an alternative, strain engineering has been identified as one of the most promising routes to tune the band gap since it is also efficacious for single layers.[6] If the band gap of GaX monolayer can be tuned in a controlled fashion, then a wide range of tunable nanodevices can be fabricated.

Our goal in the present work is to explore, for the first time, the electronic behaviors and the low-loss EELS of monolayer, bilayer, four-layer, and bulk configurations of GaX, as well as the effect of mechanical strain on the electronic properties of GaX monolayer. Particular attention will be focused on the following questions: (i) Is there a significant band gap change from the multilayer to single layer? (ii) Can EELS be used to effectively show the number of the layers in a sheet of GaX? (iii) Will the mechanical modulation of strain be a powerful and viable pathway to substantially engineer the electronic behaviors of GaX monolayer? A practical means of doing so would pave the way to a new generation of controllable and tunable electronic devices accessible to a broad spectrum of researchers worldwide.

II. Computational methods

Our calculations on all configurations are based on density functional theory (DFT) using the generalized gradient approximation (GGA)[32] in the form proposed by Perdew, Burke, and Ernzerhof (PBE) as implemented in the Vienna *ab initio* simulation package (VASP) code.[33] Note that the weak van der Walls interaction between the layers plays an important role in determining the interlayer distance for the multilayer GaX as well as the bulk GaX; the van der Walls interaction arises from dynamical correlations between fluctuating charge distributions and cannot be described by the PBE functional.[34,35] Consequently, for the bilayer, four-layer, and bulk configurations of GaX, the van der Walls interaction by adding a semi-empirical dispersion potential (D) to the conventional Kohn–Sham DFT energy, through a pair-wise force field following Grimme's DFT-D2 method,[36] is incorporated to better describe the non-bonding interactions between the layers. The projected augmented wave (PAW) method[37,38] with a plane-wave basis set is used. For all structures of GaX, we perform the calculations using a unit cell. The periodic boundary conditions and a vacuum space of 17 Å along the z direction are applied, which is enough to separate the interaction among the periodic images. The Monkhorst–Pack special k-point meshes[39] of $15 \times 15 \times 1$ and $15 \times 15 \times 5$ are used for the unit cell of multilayer (*i.e.*, monolayer, bilayer, and four-layer) and bulk GaX, respectively, to sample the Brillouin zone for geometry optimization and self-consistent electronic structure calculation for band dispersion. All of the structures were relaxed using the conjugated gradient method without any symmetric constraints. The energy cutoff and convergence criteria for energy and force are set to be 450 eV, 1×10^{-4} eV, and 0.02 eV Å^{-1}, respectively. The accuracy of our simulation procedure is tested through a comparison of the calculated lattice constant (GaS: $a = b = 3.583$ Å, $c = 15.531$ Å; GaSe: $a = b = 3.751$ Å, $c = 15.948$ Å) and the experimental value (GaS: $a = b = 3.587$ Å, $c = 15.492$ Å; GaSe: $a = b = 3.752$ Å, $c = 15.950$ Å) for the bulk phase of GaX,[40,41] which shows good agreement.

III. Results and discussion

As a starting point for examining the GaX monolayer, we first studied the geometric properties of the bulk phase of GaX. Bulk GaX is a layered semiconductor consisting of weakly van der Waals bound X–Ga–Ga–X slabs. As illustrated in Fig. 1a, in each slab, every Ga atom is covalently bound to three X atoms and another Ga atom, giving rise to a trigonal prismatic arrangement.

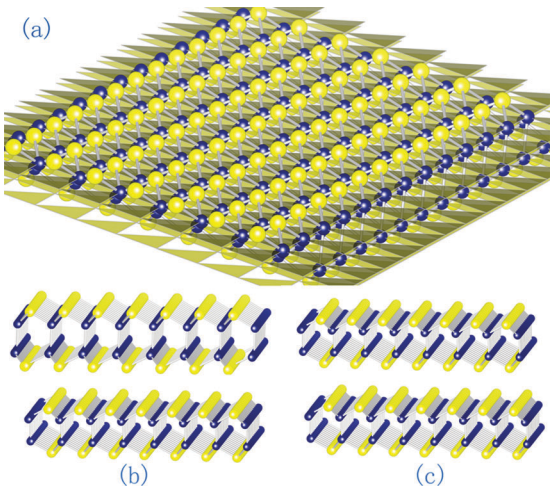

Fig. 1 (a) Crystal structure of GaX monolayer. Structure of (b) GaS and (c) GaSe bilayer with Ga and X atoms are shown by blue and yellow (smaller) spheres, respectively.

The weak inter-slab interaction allows the formation of several polytypes,[42] due to the possibility of different stacking sequences of the X–Ga–Ga–X slabs along the *c* direction. While GaS favors the β structure, the ε structure is the most common polytype for GaSe,[22,43] see Fig. 1b and c, respectively. The optimized lattice parameters are listed in Table 1. When bulk GaX is exfoliated, 2D sheets with all number of slabs are formed. In this work, to investigate the electronic properties of GaX layered structures with respect to the slab thickness, three configurations, *i.e.*, monolayer, bilayer and four-layer, of 2D sheets of GaX are considered. The equivalent lattice parameters of these 2D configurations are depicted in Table 1. From Table 1, one can see that these configurations exhibit similar crystal structures to that of the corresponding layers in bulk GaX, except for some parameters variation. In detail, lattice constant, Ga–X bond length, and X–X bond length are larger in the case of the monolayer than in the rest. This phenomenon arises from the lack of interlayer interactions in monolayer.

Fig. 2 displays the band structures of GaX upon reducing the numbers of layers from bulk to four-layer, bilayer, and monolayer. The corresponding lowest energy transition and direct lowest energy transition are listed in Table 1. For GaS, the bulk compound shows an indirect gap of 1.605 eV consisting of the valence band maximum (VBM) (horizontal dotted lines), which are set to zero in order to clarify the band gap, at the Γ point and the conduction band minimum (CBM) at the *M* points. The optical direct gap situates at the Γ point, yielding a band gap of 1.785 eV, which is only slightly larger than the indirect gap. As the number of the layers reduces, the VBM moves toward the *M* and *K* points while the CBM stays at the *M* point (independent of the slab thickness), thus indirect band gaps are obtained at all the layers. When one moves across the series from four-layer to bilayer and monolayer, the indirect gap get continuously enlarged significantly. Note that up to monolayer from the bulk, the direct gap remains between the Γ point of VBM and CBM with enhancing the gap energy. From the projection analysis, the bands near the Fermi level are derived from the s-states and p-states. In detail, the valence bands near the Fermi level are predominantly derived from the S p_z orbitals;

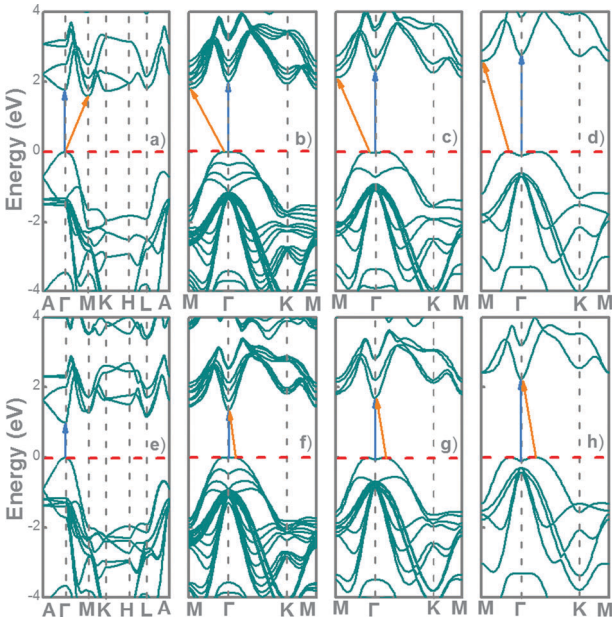

Fig. 2 Band structures of GaX, with the upper row corresponding to GaS from the (a) bulk to (b) four-layer, (c) bilayer, and (d) monolayer; and the lower row corresponding to GaSe from the (e) bulk to (f) four-layer, (g) bilayer, and (h) monolayer. The horizontal dashed red lines indicate the Fermi level. The orange solid arrows indicate the lowest energy transition, and the blue solid arrows indicate the direct lowest energy transition.

while the conduction bands near the Fermi level originate from mostly S s and Ga s orbitals with weak contribution of the S p_z orbitals.

Similar to GaS, bulk GaSe is also semiconducting, but with a direct band gap located at the Γ point, see Fig. 2e, which agrees with previous calculations.[22,43,44] With decreasing the number of layers, as illustrated in Fig. 2, one can immediately see that a progressive confinement-induced shift is the direct gap at the Γ point from the bulk value of 0.995 eV to over 2.352 eV for GaSe monolayer. As a consequence of these different variation properties, for the first time, the GaSe crystals are found to exhibit a rather surprising crossover from a direct- to an indirect-gap semiconductor in the 2D sheet limit. These findings are in contrast to those for of the well studied MoS_2,[45] in which the indirect band gap, which lies below the direct gap in the bulk materials, shifts upwards in energy by more that 0.6 eV with decreasing thickness, leading to a crossover from indirect- to direct-gap materials in the limit of the single monolayer. The overall features of the present calculated band structures for all configurations of 2D GaSe sheets are quite consistent with each other. When passing from four-layer to monolayer, the VBM shifts along the Γ–*M* and Γ–*K* lines. Interestingly, the indirect gap increases to 2.252 eV in the GaSe monolayer, which is only 0.1 eV lower than the direct band gap. However, the energy difference between the direct gap and indirect gap for GaSe monolayer is so small that electrons can easily transfer between this minimum with a small amount of thermal energy. GaSe quantum dots and nanowire display a drastic influence of quantum confinement on their electronic properties.[46,47]

Table 1 Calculated lattice constant (*a*, in Å), buckled height between two X atom planes in one slab (*D*, in Å), Ga–X bond length (d_{Ga-X}, in Å), X–X bond length (d_{Ga-G}, in Å), the lowest energy transition (LET, in eV), and the direct lowest energy transition (DLET, in eV) for optimized monolayer, bilayer, four-layer, and bulk configurations of GaX

		a	*D*	d_{Ga-X}	d_{Ga-Ga}	LET	DLET
GaS	Monolayer	3.640	4.659	2.369	2.474	1.605	1.785
	Bilayer	3.582	4.660	2.348	2.440	1.819	2.035
	Four-layer	3.582	4.656	2.346	2.440	2.141	2.368
	Bulk	3.583 (3.587[a])	4.661	2.347	2.444	2.597	2.882
GaSe	Monolayer	3.821	4.827	2.501	2.470	0.995	0.995
	Bilayer	3.749	4.820	2.471	2.432	1.341	1.351
	Four-layer	3.749	4.815	2.471	2.430	1.689	1.743
	Bulk	3.751 (3.752[a])	4.823	2.473	2.434	2.252	2.352

[a] Ref. 40 and 41.

Aside from these intriguing features, other virtues GaX monolayer possesses are the thermal stability and the absence of dangling bonds, rendering GaSe monolayer promising for nanophotonic devices.

As just discussed, the properties of these materials vary distinctly with the number of layers in a sheet; thus EELS may be a powerful technique to identify the thickness of the specimens. As a first step in verifying this exception, we probe the EELS of monolayer, bilayer, four-layer, and bulk configurations of GaX. To set the stage, the EELS loss function is computed by taking the imaginary part of the inverse of the in-plane component of the dielectric tensor, $\varepsilon_{\alpha\beta}$, in the random phase approximation; the function is expressed in terms of the following equation:

$$\text{Loss Energy}\,(\omega) = \frac{\varepsilon^{(2)}_{\alpha\beta}(\omega)}{\varepsilon^{(1)2}_{\alpha\beta}(\omega) + \varepsilon^{(2)2}_{\alpha\beta}(\omega)}$$

where $\varepsilon^{(1)}_{\alpha\beta}(\omega)$ and $\varepsilon^{(2)}_{\alpha\beta}(\omega)$ are the real part and the imaginary part of the frequency dependent dielectric tensor, respectively. The imaginary part of the dielectric tensor is obtained according to

$$\varepsilon^{(2)}_{\alpha\beta}(\omega) = \frac{4\pi^2 e^2}{\Omega}\lim_{q\to 0}\frac{1}{q^2}\sum_{c,v,\boldsymbol{k}} 2\omega_{\boldsymbol{k}}\delta(\varepsilon_{c\boldsymbol{k}} - \varepsilon_{v\boldsymbol{k}} - w) \times \langle u_{c\boldsymbol{k}+e_\alpha q}|u_{v\boldsymbol{k}}\rangle\langle u_{c\boldsymbol{k}+e_\beta q}|u_{v\boldsymbol{k}}\rangle^*$$

and the real part of the dielectric tensor is given by the Kramers–Kronig transformation[48,49]

$$\varepsilon^{(1)}_{\alpha\beta}(\omega) = 1 + \frac{2}{\pi}\int_0^\infty \frac{\varepsilon^{(2)}_{\alpha\beta}(\omega')\omega'}{\omega'^2 - \omega^2}\mathrm{d}\omega'.$$

Here, the indices c, indices v, $u_{\boldsymbol{k}}$, ω_k, Ω, and e_α refer to the conduction band states, the valence band states, an eigenstate with wave vector $\boldsymbol{k}$, the k-point weights (which are defined such that they sum to 1), the volume of the unit cell, and the unit vectors for the three Cartesian directions, respectively. The factor 2 before the weights accounts for the fact that a spin degenerate system is considered. A large number of empty conduction band states (three times than the number of valence bands) are included for the summation in the second equation.

With this model in hand, one can calculate the EELS of the monolayer, bilayer, four-layer, and bulk configurations of GaX; the corresponding results are depicted in Fig. 3. To ensure the accuracy of our simulation and compare with the spectrum of the semiconducting GaX, we also investigate the EELS spectrum of the insulting h-BN with different thickness. As Fig. 3 illustrates, the EELS spectrum for all configurations consists of two prominent plasmon peaks: (i) one plasmon peak appears above the loss energy of 8 eV [$\pi + \sigma$ plasmon peak], (ii) the other plasmon peak appears below the loss energy of 8 eV [π plasmon peak]. As Fig. 3a displays, we find that the EELS for bulk h-BN

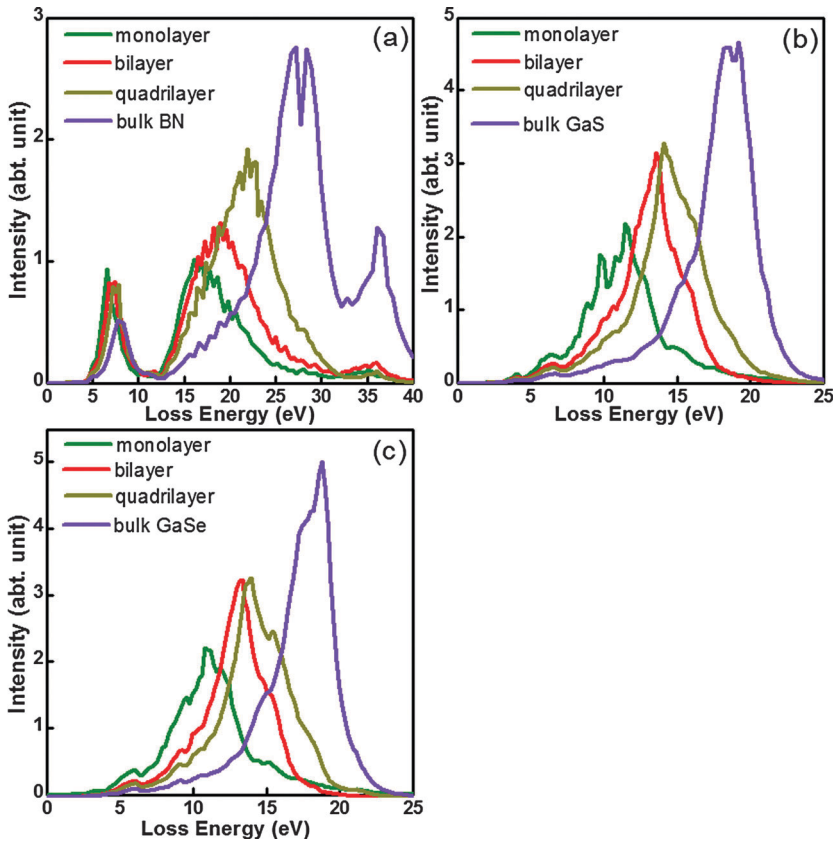

Fig. 3 The calculated electron energy loss spectroscopy of monolayer, bilayer, four-layer, and bulk configurations of (a) BN, (b) GaS and (c) GaSe.

is quantitatively consistent with the recent experimental measured[2] and the theoretically calculated[19] EELS results. On the other hand, on comparing the results presented in Fig. 3, one can clearly see that, for *h*-BN, the EELS spectrum displays π and π + σ plasmon peaks specifically; while for GaX materials, the π plasmon peak is not well-defined. This discrepancy probably arises from the difference, in the overlap of the π and σ valence bands, between the *h*-BN and the GaX materials.[2,19]

If the EELS are to detect the number of the layers in a GaX sheet, then, at a minimum, it should be able to distinguish a thick sheet, like bulk, from a thin sheet, like monolayer. This criterion leads us to focus on the EELS of the bulk and monolayer configurations of GaX. Our calculations reveal that, for GaS (GaSe), the π + σ plasmon peak locates at the loss energy of around 18.6 eV (18.4 eV) for the bulk phase; while this peak shifts to 10.8 eV (10.6 eV) for the case of monolayer. These results imply that EELS satisfies the criteria. We wish to point out that this might be feasible to achieve the identification of a thin sheet from a thick sheet. However, to be a practical and powerful tool, the EELS should be able to locate the number of a sheet sensitively. In this case, the EELS should vary drastically from four-layer to bilayer and monolayer configurations of GaX. As Fig. 3 illustrates, more remarkably, there is a clear π + σ plasmon peak at the loss energy of 13.6 eV (13.2 eV) and 14.3 eV (14.1 eV), respectively, for the bilayer and four-layer configurations of GaS (GaSe), which exhibits a significant red-shift of 2.8 eV (2.6 eV) and 3.5 eV (3.5 eV) when compared to the case of the monolayer configuration of GaS (GaSe). Besides these features, it is worth highlighting that the intensity of the plasmon peak also changes as a function of slab thickness. In detail, the π + σ plasmon peak decreases upon reducing the numbers of layers from bulk to four-layer, bilayer, and monolayer configurations of GaX. As addressed in Fig. 3a, a similar trend in the evolution of the EELS is also observed in the insulting *h*-BN. Based on these results, one can establish that the determination of layer thickness by investigating the EELS spectrum is viable, independent of the semiconducting or the insulting nature of the materials.

According to the analysis above, one can establish that GaX monolayer is technologically promising. Yet materials with suitable electric properties to realize most electronic devices are desirable. Moreover, advanced applications often require materials with tunable and reversible electronic properties which can be deliberately modulated by external control parameters, which is central to practical applications.[26] Awareness of the strain effect is always important in nanosystems, quite naturally, it is tempting to investigate whether the mechanical deformation can be a viable pathway to substantially engineer the electronic behaviors of GaX monolayer. To verify this exception, we appeal to three types of mechanical modulation of strain. In the first case, strain is simulated by variation of the lattice along the *a* axis for constant *b* (denoted as strain I, as illustrated in Fig. 4). For the second, we consider the biaxial lattice expansion, where the crystal structure is expanded in the *ab* plane with same magnitude of strain (denoted as strain II, as illustrated in Fig. 4). In the third case, strain is applied by expanding and compressing the GaX monolayer in the *a* and *b* directions, respectively, with same magnitude of strain (denoted as strain III, as illustrated in Fig. 5). It should be noted that, for all the three types of strain, we apply strain by

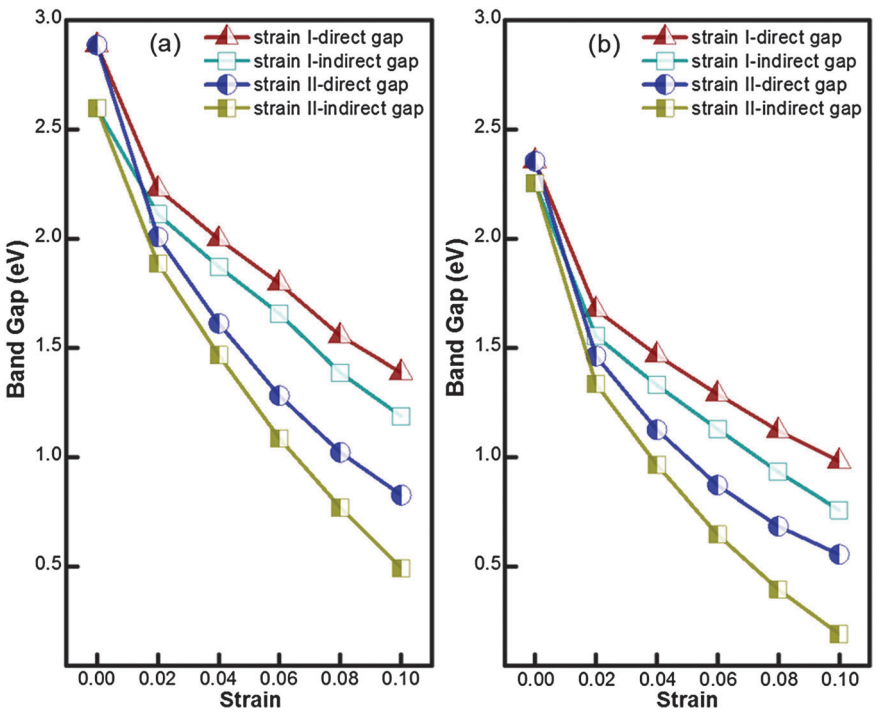

Fig. 4 The band gap of the monolayer configurations for (a) GaS and (b) GaSe *versus* different strain conditions. For (a) and (b), strain I is simulated by variation of the lattice along the *a* axis for constant *b* and strain II is simulated by variation of the lattice along the *ab* plane.

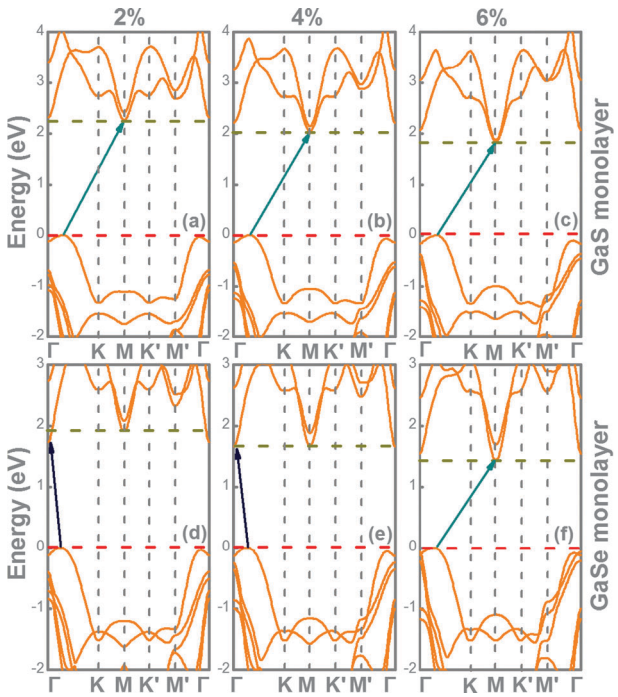

Fig. 5 Band structures of the monolayer configurations of GaX, with the upper row corresponding to GaS with strain III of (a) 2%, (b) 4%, and (c) 6%; and the lower row corresponding to GaSe with strain III of (d) 2%, (e) 4%, and (f) 6%. The horizontal dashed red lines indicate the Fermi level. The solid arrows indicate the lowest energy transition.

changing the in-plane (a and b) cell parameters, relaxing the structure along the c-axis (the direction perpendicular to the sheets), since on applying an in-plane strain, a deformation in the perpendicular (z) direction is likely. From Fig. 4 and 5, one can see that the variations in the band gap with respect to strain applied through various approaches alter slightly with the change in chalcogenides.

As Fig. 4 addresses, on application of strain I and strain II, the direct and indirect band gaps labeled in Fig. 2d and h decrease monotonically in energy. In particular, for GaS monolayer under strain I and strain II, the indirect band gap character retains up to the strain of 10%, with the lowest energy transition stays corresponds to $\Gamma M(K)$–M and the shortest direct transition corresponds to Γ–Γ. Similar features are also found in the case of GaSe monolayer: the lowest energy transition corresponds to $\Gamma M(K)$–Γ and the shortest direct transition corresponds to Γ–Γ. With increasing strain I and strain II, our calculations reveal that the band gap is substantially quenched due to the remarkable down-shift of the CBM at Γ and M, and conversely, the VBM remains almost intact at the Γ–$M(K)$ direction. As a result, the nature of band gap for GaX monolayer under both strain conditions is kept consistent with the unstrained cases. On the other hand, it is also worth emphasizing that a significant diversity in the magnitude of band gap variation can be seen with the change in moving from strain I to strain II, *i.e.*, the band gap decrease for strain I is not as steep as for the case of strain II. Explanation of this interesting diversity as well as the strain-depend band gap evolution is sought in the particular composition of the valence and the conduction bands near the Fermi level. Based on the projection analysis, the valence bands Fermi level are dominated by the X p_z states, while the conduction bands near the Fermi level are mainly composed of X s, X p_z and Ga s states. Thus the band gap is determined by the covalent sp_z hybridization between the Ga and X atoms. Evidently, the sp_z hybridization depends sensitively on the strain, due to the fact that the distance between the Ga and X atoms ($d_{Ga–X}$) increases with increasing strain I and strain II, and the elongation of the $d_{Ga–X}$ results in the reduction in the sp_z hybridization. Consequently, the increasing of strain I and strain II would lead to the reduction in the sp_z hybridization, thus giving rise to the monotonic decrease of the band gap. Based on this mechanism, the significant diversity in the steep variation of band gap with different strain types can be easily understood. Knowing that the elongation of the $d_{Ga–X}$ induced by increasing strain II is larger than that induced by increasing strain I, the reduction of the sp_z hybridization induced by increasing strain II would be larger than that induced by increasing strain I, thus resulting in the relative larger steep descend of the band gap variation in the strain II case with respect to the case of strain I.

Besides tensile strain, shear strain (strain III) is also responsible for the band gap modification. Thus, we now turn our attention to the effect of strain III on the electronic properties of GaX monolayer. Closer examination of the band structures of the strained GaS monolayer (see Fig. 5a–c) shows that application of strain III leads to downward shifting of the conduction band around the Γ and M points, but the downward shifting of the conduction band at the Γ point is relatively slow. This leads to a shift of the CBM from the Γ to M points (see Fig. 5a). As the VBM around the Γ and K line does not experience a similar shift and, on the contrary, stays totally unaffected by the strain III, the indirect band gap is kept and the band gap is significantly decreased. On the other hand, on examining GaX exhibiting atoms heavier than S, *i.e.*, GaSe monolayer, we find the diffuse nature of this chalcogenide atoms remarkably affects its response to strain (see Fig. 5d–f). Our results demonstrate that for GaSe, the band gap decreases relatively slowly and larger amounts of tensile strain are required to obtain the transition which corresponds to Γ–M. For instance, this transition is achieved faster, namely, at low strain (2%) in GaS monolayer as compared to that of GaSe monolayer, where strain of more than 6% is required to obtain the shift. Accordingly, the band gap of GaX monolayer can be efficiently modulated with increasing different strain. The rapid variation of band gap under strain may be useful for applications in nanodevices, such as a mechanical switch.

IV. Conclusions

In summary, based on the density functional theory computations, we systematically investigated the electronic behaviors and the low-loss EELS of monolayer, bilayer, four-layer, and bulk configurations of GaX, as well as the effect of mechanical strain on the electronic properties of GaX monolayer. Our findings

can be summarized in three main points: (1) For the first time, we demonstrate that, different from transition-metal dichalcogenides which exhibit crossover from indirect- to direct-gap materials in the limit of the single monolayer, the GaSe changes its electronic properties from a direct semiconductor in the bulk phase to an indirect semiconductor in the monolayer; while for GaS, it retains its indirect gap nature with the change from the bulk to the monolayer phases. Nevertheless, for the GaX monolayer, the difference between direct and indirect gaps is so small that electrons can easily be transferred between this minimum with a small amount of thermal energy, an interesting phenomenon with potential application in field-effect transistors. (2) Interestingly, owning to the strong surface effects, the electronic and dielectric properties of GaX vary drastically with the number of layers in a sheet. In detail, the band gap increases from multilayer-to-single layer and electron energy loss spectra shift towards larger wavelength with a substantial decrease in layer thickness. Based on these results, one can establish that the determination of layer thickness by investigating the EELS spectrum is viable. (3) Aside from these features, more specifically, we find that the band gap of GaX monolayer can be widely tuned by applying mechanical deformation, making them not only potential alternatives to graphene, as they could also define a new range of tunable nanodevices. In particular, upon application of biaxial tensile strain, the band gap decreases relatively significantly compared to the other two types of strain, resulting from the particular sp_z hybridization between the Ga and X atoms.

Our results give insightful prospects for understanding the newly synthesized two-dimensional nanosheets and paving the way to a new generation of controllable and tunable electronic devices accessible to a broad spectrum of researchers worldwide.

Acknowledgements

This work is supported by the National Basic Research Program of China (973 program, 2013CB632401), National Science Foundation of China under Grant 11174180 and the Fund for Doctoral Program of National Education 20120131110066, Natural Science Foundation of Shandong Province under Grant number ZR2011AM009, and the Ministry of Education Academic award for postgraduates. We also thank the National Supercomputer Center in Jinan for providing high performance computation.

References

1 K. S. Novoselov, A. K. Geim, S. V. Morozov, D. Jiang, Y. Zhang, S. V. Dubonos, I. V. Grigorieva and A. A. Firsob, *Science*, 2004, **306**, 666.
2 K. S. Novoselov, E. McCann, S. V. Morozov, V. I. Falko, M. I. Katsnelson, U. Zeitler, D. Jiang, F. Schedin and A. K. Geim, *Nat. Phys.*, 2006, **2**, 177.
3 Y. D. Ma, Y. Dai, M. Guo, C. W. Niu and B. B. Huang, *J. Phys. Chem. C*, 2012, **116**, 12977.
4 A. J. Du, S. Sanvito, Z. Li, D. W. Wang, Y. Jiao, T. Liao, Q. Sun, Y. H. Ng, Z. H. Zhu, R. Amal and S. C. Smith, *J. Am. Chem. Soc.*, 2012, **134**, 4393.
5 Q. Tang, Z. Zhou and P. W. Shen, *J. Am. Chem. Soc.*, 2012, **134**, 16909.
6 Y. D. Ma, Y. Dai, M. Guo, C. W. Niu, Y. T. Zhu and B. B. Huang, *ACS Nano*, 2012, **6**, 1695.
7 S. Stankovich, D. A. Dikin, G. H. B. Dommett, K. M. Kohlhaas, E. J. Zimney, E. A. Stach, R. D. Piner, S. T. Nguyen and R. S. Ruoff, *Nature*, 2006, **442**, 282.
8 K. M. Fair, X. Y. Cui, L. Li, C. C. Shieh, R. K. Zheng, Z. W. Liu, B. Delley, M. J. Ford, S. P. Ringer and C. Stampfl, *Phys. Rev. B: Condens. Matter Mater. Phys.*, 2013, **87**, 014102.
9 D. C. Elias, R. R. Nair, T. M. G. Mohiuddin, S. V. Morozov, P. Blake, M. P. Halsall, A. C. Ferrari, D. W. Boukhvalov, A. K. Geim and K. S. Novoselov, *Science*, 2009, **323**, 610.
10 J. Zhou, M. M. Wu, X. Zhou and Q. Sun, *Appl. Phys. Lett.*, 2009, **95**, 103108.
11 Y. D. Ma, Y. Dai, M. Guo, C. W. Niu, Z. K. Zhang and B. B. Huang, *Phys. Chem. Chem. Phys.*, 2012, **14**, 3651.
12 Y. F. Li, F. Y. Li and Z. F. Chen, *J. Am. Chem. Soc.*, 2012, **134**, 11269.
13 Y. D. Ma, Y. Dai, M. Guo, C. W. Niu, J. B. Lu and B. B. Huang, *Phys. Chem. Chem. Phys.*, 2011, **13**, 15546.
14 B. L. Evans, in *Physics and Chemistry of Materials with Layered Structures, Electrical and Optical Properties*, ed. P. A. Lee, D. Reidel Publish, Boston, 1976, vol. 4.
15 V. Grasso and G. Mondio, in *Electronic Structure and Electronic Transitions in Layered Materials*, ed. V. Grasso, D. Reidel Publish, Dordrecht, 1986.
16 D. J. Late, B. Liu, H. S. S. R. Matte, C. N. R. Rao and V. P. Dravid, *Adv. Funct. Mater.*, 2012, **22**, 1894.
17 D. J. Late, B. Liu, J. Luo, A. Yan, H. S. S. R. Matte, M. Grayson, C. N. R. Rao and V. P. Dravid, *Adv. Mater.*, 2012, **24**, 3549.
18 P. A. Hu, Z. Z. Wen, L. F. Wang, P. H. Tan and K. Xiao, *ACS Nano*, 2012, **6**, 5988.
19 P. Johari and V. B. Shenoy, *ACS Nano*, 2012, **6**, 5449.
20 Y. G. Zhou, Z. G. Wang, P. Yang, X. T. Zu, L. Yang, X. Sun and F. Gao, *ACS Nano*, 2012, **6**, 9727.
21 S. Nüsse, P. H. Bolivar, H. Kurz, F. Levy, A. Chevy and O. Lang, *Phys. Rev. B: Condens. Matter Mater. Phys.*, 1997, **55**, 4620.
22 Z. Y. Zhu, Y. C. Cheng and U. Schwingenschlögl, *Phys. Rev. Lett.*, 2012, **108**, 266805.
23 J. N. Coleman, M. Lotya, A. Neill, S. D. Bergin, P. J. King, U. Khan, K. Young, A. Gaucher, S. De, R. J. Smith, I. V. Shvets, S. K. Arora, G. Stanton, H. Y. Kim and K. Lee, *et al.*, *Science*, 2011, **331**, 568.
24 J. B. Sun, J. B. Hannon, R. M. Tromp, P. Johari, A. A. Bol, V. B. Shenoy and K. Pohl, *ACS Nano*, 2010, **4**, 7073.
25 P. Johari and V. B. Shenoy, *ACS Nano*, 2011, **5**, 5903.
26 D. Venkateshvaran, M. Althammer, A. Nielsen, S. Geprags, M. S. Ramachandra Rao, S. T. B. Goennenwein, M. Opel and R. Gross, *Phys. Rev. B: Condens. Matter Mater. Phys.*, 2009, **79**, 134405.

27 D. Chiba, M. Yamanouchi, F. Matsukura and H. Ohno, *Science*, 2003, **301**, 943.
28 H. Tanaka, J. Zhang and T. Kawai, *Phys. Rev. Lett.*, 2001, **88**, 027204.
29 Z. H. Ni, T. Yu, Y. H. Lu, Y. Y. Wang, Y. P. Feng and Z. X. Shen, *ACS Nano*, 2008, **2**, 2301.
30 E. McCann, *Phys. Rev. B: Condens. Matter Mater. Phys.*, 2006, **74**, 161403.
31 A. Ramasubramaniam, D. Naveh and E. Towe, *J. Electrochem. Soc.*, 2011, **84**, 205325.
32 J. P. Perdew, K. Burke and M. Ernzerhof, *Phys. Rev. Lett.*, 1996, **77**, 3865.
33 G. Kresse and J. Furthmuller, *Phys. Rev. B: Condens. Matter Mater. Phys.*, 1996, **54**, 11169.
34 S. Bhattacharyya and A. K. Singh, *Phys. Rev. B: Condens. Matter Mater. Phys.*, 2012, **86**, 075454.
35 Y. D. Ma, Y. Dai, M. Guo and B. B. Huang, *Phys. Rev. B: Condens. Matter Mater. Phys.*, 2012, **85**, 235448.
36 S. Grimme, *J. Comput. Chem.*, 2006, **27**, 1787.
37 P. E. Bloochl, *Phys. Rev. B: Condens. Matter Mater. Phys.*, 1994, **50**, 17953.
38 G. Kresse and D. Joubert, *Phys. Rev. B: Condens. Matter Mater. Phys.*, 1999, **59**, 1758.
39 H. J. Monkhorst and J. D. Pack, *Phys. Rev. B: Condens. Matter Mater. Phys.*, 1976, **13**, 5188.
40 A. Kuhn, A. Chevy and R. Chevalier, *Acta Crystallogr., Sect. B: Struct. Crystallogr. Cryst. Chem.*, 1976, **32**, 983.
41 A. Kuhn, A. Chevy and R. Chevalier, *Phys. Status Solidi A*, 1975, **31**, 469.
42 J. Terhell, V. Brabers and G. van Egmond, *J. Solid State Chem.*, 1982, **41**, 97.
43 G. L. Belenki, E. Y. Salaev and R. A. Sulemanov, *Sov. Phys.–Usp.*, 1988, **31**, 434.
44 D. Errandonea, A. Segura, F. J. Manjon, A. Chevy, E. Machado, G. Tobias, P. Ordejon and E. Canadell, *Phys. Rev. B: Condens. Matter Mater. Phys.*, 2005, **71**, 125206.
45 K. F. Mak, C. G. Lee, J. Hone, J. Shan and T. F. Heinz, *Phys. Rev. Lett.*, 2010, **105**, 136805.
46 A. Balitskii, E. Borowiak-Palen and W. Konicki, *Cryst. Res. Technol.*, 2011, **46**, 417.
47 V. Chikan and D. F. Kelley, *Nano Lett.*, 2002, **2**, 141.
48 M. Gajdos, K. Hummer, G. Kresse, J. Furthmuller and F. Bechstedt, *Phys. Rev. B: Condens. Matter Mater. Phys.*, 2006, **73**, 045112.
49 H. Ehrenreich and M. H. Cohen, *Phys. Rev.*, 1959, **115**, 786.